# Multihole water oxidation catalysis on hematite photoanodes revealed by *operando* spectroelectrochemistry and density functional theory

Camilo A. Mesa,[1†] Laia Francàs,[1†] Ke R. Yang,[2] Pablo Garrido, [2,3] Ernest Pastor,[1] Yimeng Ma,[1] Andreas Kafizas,[1] Timothy E. Rosser,[4] Matthew T. Mayer,[5,6] Erwin Reisner,[4] Michael Grätzel,[5] Victor S. Batista,[2*] James R. Durrant[1*]

1. Molecular Sciences Research Hub and Centre for Plastic Electronics, Imperial College London, White City Campus, London W12 0BZ, United Kingdom
2. Department of Chemistry and Energy Sciences Institute, Yale University, New Haven, Connecticut 06520-8107, United States
3. Institute of Chemical Research of Catalonia (ICIQ), Avinguda Països Catalans 16, E-43007 Tarragona, Spain
4. Christian Doppler Laboratory for Sustainable SynGas Chemistry, Department of Chemistry, University of Cambridge, Lensfield Road, Cambridge CB2 1EW, United Kingdom
5. Institut des Sciences et Ingénierie Chimiques, Ecole Polytechnique Fédérale de Lausanne, Station 6, CH-1015 Lausanne, Switzerland
6. Helmholtz-Zentrum Berlin für Materialien und Energie GmbHHahn-Meitner-Platz 1, 14109 Berlin, Germany

[†]These authors contributed equally to this manuscript

*Corresponding authors: Victor.batista@yale.edu, j.durrant@imperial.ac.uk

**Summary**

Water oxidation is the key kinetic bottleneck of photoelectrochemical devices for fuel synthesis. Despite advances in the identification of intermediates, elucidating the catalytic mechanism of this multi-redox reaction on metal-oxide photoanodes remains a significant experimental and theoretical challenge. Here we report an experimental analysis of water oxidation kinetics on four widely studied metal oxides, focusing particularly upon hematite. We observe that hematite is able to access a reaction mechanism third order in surface hole density, assigned to equilibration between three surface holes and M(OH)-O-M(OH) sites. This reaction exhibits a remarkably low activation energy ($E_a$ ~ 60 meV). Density functional theory is employed to determine the energetics of charge accumulation and O-O bond formation on a model hematite 110 surface. The proposed mechanism shows parallels with the function of oxygen evolving complex of photosystem II, and provides new insights to the mechanism of heterogeneous water oxidation on a metal oxide surface.

The light driven oxidation of water by Photosystem II (PS II) is one of the most remarkable catalytic reactions in biology. It provides the reducing electrons for photosynthetic carbon dioxide reduction and releases molecular oxygen, which has generated our aerobic atmosphere. Natural photosynthesis is widely regarded as an inspiration behind the development of artificial photosynthetic systems to harness sunlight and split water into molecular oxygen and hydrogen, or reduce carbon dioxide to carbon based molecular fuels.[1–4] However, it is often unclear whether natural photosynthetic systems exhibit molecular scale blueprints and mechanisms, which can help guide the development of artificial systems. Most studies of heterogeneous and homogeneous chemical water oxidation to date have focused on optimising catalytic turn over frequencies and minimising overpotentials, or long term

stabilities.[5–9] Mechanistic studies of heterogeneous water oxidation have focused particularly on the identification of reaction intermediates.[10] In the study herein, we take an alternative approach by employing an experimental rate law analysis of water oxidation on metal oxide surfaces under a range of conditions and we complement these kinetic studies with density functional theory (DFT) calculations of a simple molecular analogue for one of these oxides to propose a model for water oxidation on such surfaces.

In electrocatalytic systems, the kinetics of catalysis are often probed from analyses of current / potential (J/V) characteristics, often referred to, for metallic electrodes or defect free semiconductors (*i.e.*: with sharp band edges), as Tafel analyses.[11] However, for non-ideal electrodes, such as semiconductors with multiple redox states and / or non-ideal densities of conduction / valence band states, the interpretation of such J/V data is more complex. The rate of reaction in semiconductor electrodes is often primarily determined by the densities of surface conduction band electrons (valence band holes), or of reduced (oxidized) states of the catalyst.[12] However, for non-ideal semiconductors, these densities are often difficult to determine from J/V analyses alone. For photoelectrocatalytic systems, determination of these densities from J/V data alone is further complicated by the quasi-Fermi level splitting induced by light. As such, for many (photo)electrocatalytic systems, determination of rate laws for multi-redox reactions is a non-trivial challenge, with only limited studies reported in the literature to date.[13] Similarly, theoretical calculations have typically not addressed the dependence of the reaction rate upon surface charge density.

We have recently demonstrated, for both electrocatalytic and photoelectrocatalytic systems, that optical spectroscopy can provide a direct measurement of the densities of the states driving catalysis under operating conditions, and have employed this approach to elucidate rate laws for water and methanol oxidation and proton reduction on different (photo)electrocatalytic surfaces.[14–16] In the study herein, we employ this experimental approach to determine the dependence of the water oxidation rate constant upon temperature, pH and H/D exchange for hematite ($\alpha$-$Fe_2O_3$) photoelectrodes, thus providing key experimental data on the underlying reaction mechanism (see methods details in Supplementary Information). This experimental approach combines a transient optical absorption assay of surface hole accumulation ($h_s^+$) (see Supplementary Figure 1 for typical absorption spectra of these holes on hematite; we note these surface holes are likely to be relatively localised, with energies near the valence band edge),[16–19] with a photoelectrochemical assay of the flux of water oxidation ($J^{ph}$) which allows one to determine the rate law (Eq. 1) on such photoelectrodes:

$$J^{ph} = k_{WO} \cdot (h_s^+)^{\alpha} \qquad (1)$$

where $\alpha$ is the order of reaction with respect to the hole density and $k_{WO}$ is the corresponding water oxidation rate constant. For the studies reported herein, data were collected under strong anodic bias to supress surface recombination losses, as a function of light irradiation intensity in a three-electrode photoelectrochemical cell. Data were collected after irradiation with a 365 nm LED light pulse for 5 s, long enough to reach approximately steady-state conditions for both the surface hole and photocurrent densities.[16–18] The complete optical and electrochemical data set is available in http://zenodo.org with the identifier (10.5281/zenodo.851635). Our previous kinetic studies have demonstrated that only holes localized in the space charge layer have sufficiently long lifetimes to contribute to the quasi-steady state conditions employed, and herein we take advantage that our optical assay is sensitive only to these surface holes.[16,20]

**Results and discussion**

We start by making a quantitative comparison of the dependence of the water oxidation kinetics on the density of photogenerated charge carriers on hematite ($\alpha$-$Fe_2O_3$) and on three other photoanodes: titanium dioxide ($TiO_2$), bismuth vanadate ($BiVO_4$) and tungsten oxide ($WO_3$), as shown in Figure 1.a (for $\alpha$-$Fe_2O_3$, $TiO_2$ and $BiVO_4$ these plots are adapted from previously published data;[16–18] see Supplementary Figures 2 and 3 for optical and electrochemical characterisation). These data are plotted as log/log plots of turn over frequency (*TOF*) versus surface hole density ($h_s^+$) (where the TOF is determined from the inverse of hole transfer time constant, oxygen release TOF's would be 4 fold slower). We note that the surface hole density can be considered most simply as a measure of how close the hole quasi Fermi level approaches the valence band maximum at the surface with a higher hole density corresponding to a greater free energy driving water oxidation. All the oxides studied herein have been shown to have promising activity for water oxidation under solar irradiation and modest anodic bias and, with the exception of $WO_3$, high faradaic efficiencies.[21] Unlike PS II, their valence band maxima are all relatively deep, providing large energy offsets for water oxidation by valence band holes, as illustrated in Figure 1.c. In particular, we have previously reported that the rate of water oxidation increases with the third power of the surface hole density under one sun irradiation on $\alpha$-$Fe_2O_3$, $BiVO_4$ and $TiO_2$,[16–18] suggesting the co-operative function of three surface holes in the rate determining step (rds) of the reaction. Further data are included herein for $WO_3$ photoanodes (see Supplementary Figures 4 and 5 for $WO_3$ details). Also shown in Figure 1.b are the same data plotted more conventionally, as water oxidation flux versus surface hole density.

Figure 1.a shows that as the surface hole density is increased, the TOF is initially constant, and then increases, corresponding to a transition from a 1$^{st}$ order reaction at low surface hole densities to a faster, higher circa 3$^{rd}$ order reaction at higher hole densities, with the latter dominating under one sun irradiation. We note that the transition from 1$^{st}$ to 3$^{rd}$ order is not always quantitative. $WO_3$ photoanodes actually fit best to a 2.5 order at high hole densities showing non-unity Faradaic efficiency for water oxidation.[22] For $TiO_2$ photoanodes, the 1$^{st}$ order regime could not be resolved, and at neutral and acidic pH, we observe 2$^{nd}$ order behaviour.[18] As we have discussed previously, this unexpected biphasic behaviour, suggests distinct reaction mechanisms at different surface hole densities.[16,17] We note that a different rate law data has been reported recently for hematite based on J/V impedance data, as we discuss further in Supplementary, page 6.[23] The *TOF*s plotted in Figure 1.a ranging from 0.125 $s^{-1}$ for $\alpha$-$Fe_2O_3$ at low hole densities to 60 $s^{-1}$ for $WO_3$ at high hole densities. These values are between 1 to 2 orders of magnitude slower than that for the oxygen evolving centre (OEC) in the PS II,[24] but comparable to many homogeneous and heterogeneous chemical water oxidation catalysts.[2,21] It is apparent from this plot that the *TOF* (and therefore rate constants) for water oxidation correlate with the valence band edges (VBE) of these oxides shown in Figure 1.c. $\alpha$-$Fe_2O_3$ exhibits the slowest kinetics and least oxidising VBE while $WO_3$ the fastest kinetics and deepest VBE. More quantitatively, we observe that an increase of the VBE of 0.7 V results in a 150-fold increase in the water oxidation rate constant. Faster water oxidation kinetics can be expected to reduce losses due to kinetic competition with surface (or 'back electron hole') recombination. The variation in water oxidation kinetics we observe in Figure 1.a between these metal oxides is therefore likely to be a key reason why it is easier to achieve photocurrent onset potentials closer to the flat band for $WO_3$[25] and $TiO_2$[26] compared to $BiVO_4$[27] and $\alpha$-$Fe_2O_3$ (see Supplementary Figure 3).

We note that the surface hole densities in Figure 1.a ranges between 0.5 and 4 $nm^{-2}$, 1-2 orders of magnitude higher than densities of surface defect states typically reported for such oxides,[28,29] suggesting that any water oxidation proceeding from such defect states is unlikely to contribute significantly to data reported herein. We emphasise that this analysis contrasts with Tafel analyses of

metallic electrocatalysts, where the applied potential increases the energy of states driving catalysis, by directly measuring the density of reactive species ($h_s^+$) independently of their dependence on the applied potential. This molecular viewpoint is consistent with surface holes on such oxides being relatively localized states,[30] such that their enthalpies can be considered to be, to a first approximation, independent of surface hole density. We also emphasise that our approach can be considered more analogous to that employed for electrochemically driven molecular catalysis, as studied in catalytic Tafel plots. We note that analysis of reaction rates *vs* actual driving force of the accumulated redox species (considering the energetics of valence band tail states) would further advance our understanding of these photoelectrochemical systems.

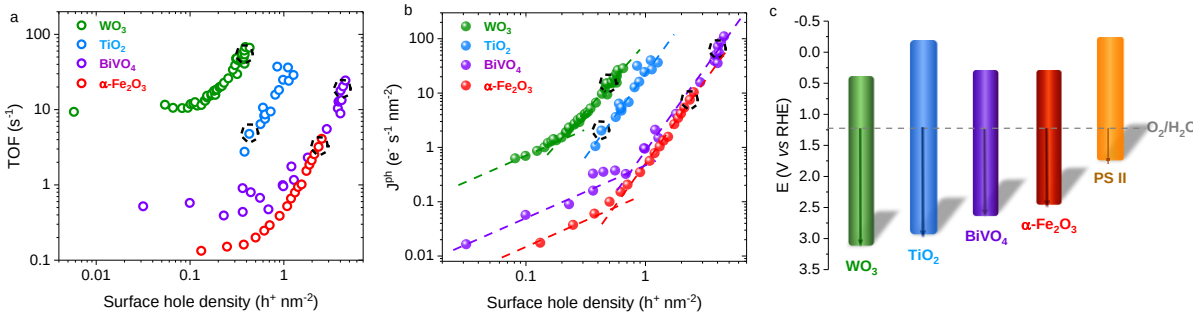


**Figure 1.** Kinetic analysis of the water oxidation reaction on metal oxide photoanodes. (a) Log/log plots of the turn over frequencies (TOF) for hole transfer to the electrolyte corresponding to water oxidation as a function of surface hole density, measured at fixed anodic bias for four metal oxide photoanodes. The black dashed circles indicate ~1 sun irradiation conditions. (b) Equivalent data plotted as rate of reaction versus surface hole density. The dashed lines correspond to fits to the rate law (Eq. 1). Conditions: $WO_3$, diffuse reflectance system (α = 1, α = 2.5), pH 3, applied potential 1.4 V vs RHE; $BiVO_4$, transmittance system (α = 1, α = 3), pH 7 at 1.7 V vs RHE;[17] α-$Fe_2O_3$, transmittance system (α = 1, α = 3), pH 13 at 1.5 V vs RHE;[16] $TiO_2$, transmittance system (α = 3) pH 13 at 1.5 V vs RHE.[18] In all cases 365 nm LED irradiation was used from 0.5% to 300% one sun and measurements were performed at 25 $^{O}$C. (c) Schematic representation of the valence band edge energy relative to the $H_2O$ oxidation redox potential (1.23 V vs RHE) of the metal oxides discussed in this paper, including the equivalent PSII energy levels for reference.

Experimental mechanistic studies of water oxidation on α-$Fe_2O_3$

We now turn to the primary focus of this paper, the use of kinetic data such as that shown in Figure 1.a to provide insight into the mechanism of water oxidation on such electrodes. This analysis focuses on hematite alone, and in particular the origin of the 3$^{rd}$ order kinetics observed under one sun illumination conditions.[16] First, we consider the temperature dependence of the 1$^{st}$ and 3$^{rd}$ order kinetics, as shown in the rate law analyses plotted in Figure 2.a. The inset to this figure shows Arrhenius analyses of these data for the 1$^{st}$ and 3$^{rd}$ order rate constants. We observe an activation energy ($E_a$) of 0.3 ± 0.05 eV for the 1$^{st}$ order mechanism, consistent with that reported from transient absorption measurements under pulsed laser excitation.[31] More importantly, we observe that the 3$^{rd}$ order reaction mechanism has a very low activation energy, $E_a$ = 0.06 ± 0.02 eV, indicating that at high hole densities, hematite is able to access a third order reaction mechanism which essentially removes all significant activation energy barriers for the water oxidation reaction. Such change in activation energy demonstrates that the hematite surface is indeed catalysing the water oxidation reaction at high surface hole densities, by lowering the activation barrier for this reaction to only 60 meV (see Supplementary Figure 6 for an alternative $E_a$ calculation).

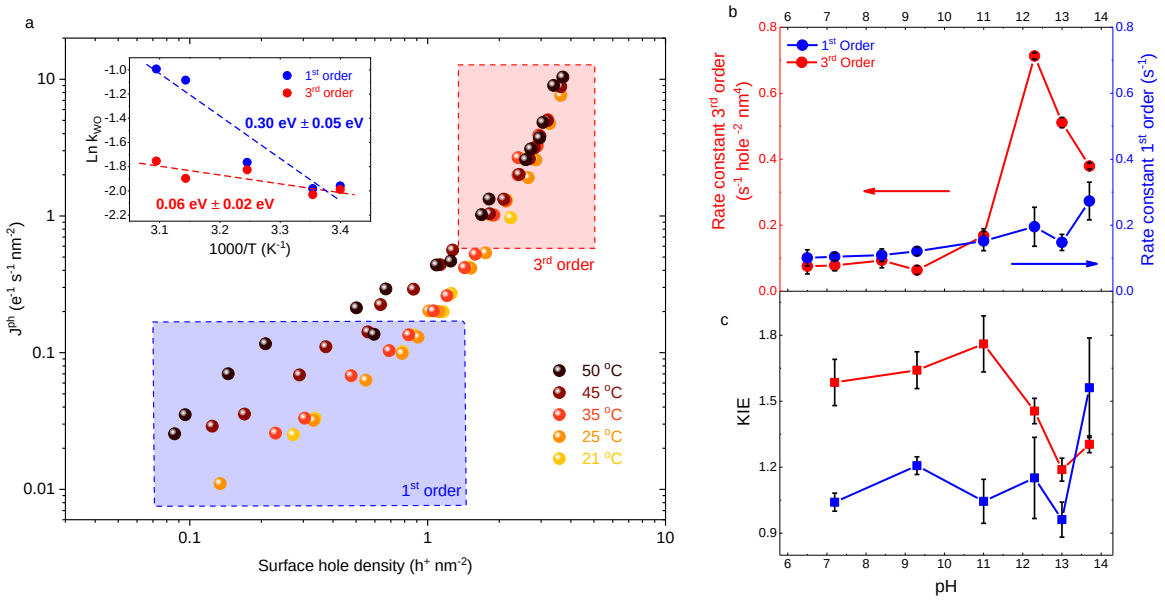


**Figure 2.** Mechanistic analyses of water oxidation on $\alpha$-$Fe_2O_3$. (a) Rate law analyses as for Figure 1.b, but at different temperatures (21 °C – 50 °C). The inset shows an Arrhenius plot of water oxidation rate constant for both the 1st and 3rd order regimes, the slopes (dotted lines) indicate the activation energies of the rate determining steps, suggesting the catalytic effect of hole accumulation on $\alpha$-$Fe_2O_3$. (b) Plots of the pH dependence of the rate constants of the 1st and 3rd order regimes. (c) Comparison of the kinetic isotope effect when $H_2O$ is replaced by $D_2O$ at different pH values for the 3rd order (red) and 1st order (blue) regimes, exhibiting no cleavage of O-H bond at the rate determining steps. (b)-(c) Error bars represent the standard deviations of linear fits of the logarithmic form of equation 1 to the full data sets shown in Supplementary Figures 8 a and b.

Before turning to discuss possible reaction mechanisms compatible with such a low activation energy, we consider two further kinetic studies probing reaction mechanism. Figure 2.b plots the pH dependence of the 1st and 3rd order water oxidation rate constants on hematite and Figure 2.c plots the kinetic isotope effect (KIE) of these rate constants for $H_2O/D_2O$ exchange as a function of pH (see also Supplementary Figure 7). It is apparent from Figure 2.b that both the 1st and 3rd order rate constants are essentially pH independent for pH values of up to 9.5, and then increase modestly (although not monotonically) for higher values of pH. The relatively weak pH dependence indicates that electrolyte hydroxides are not directly involved in the rate-determining step of either reaction. The onset of a modest increase in $k_{WO}$ above pH 9 coincides with the point of zero charge (pzc) of hematite (8-10).[32] This suggests that the increase in $k_{WO}$ above pH 9 is most likely associated with a change in the surface protonation of hematite. This also correlates with a change in the pH dependence of the photocurrent onset potential from an ideal Nernstian 60 mV/pH at acidic / neutral pH to a 100 mV/pH at alkali pH (Supplementary Figures 8 and 9).

From Figure 2.c, it is clear that the H/D KIE is small for the 1st order rate constant at pH < 14 (KIE ~ 1.1), indicating that O-H bond cleavage is not involved in the rate-determining step of this reaction. On the other hand, the 3rd order rate constant exhibits a modest secondary KIE effect, ~1.7 (expected KIE of 2.5, see DFT calculations below) from pH 7 to pH 11, decreasing to ~1.3 at more alkaline pH, which we discuss further below.

DFT calculations

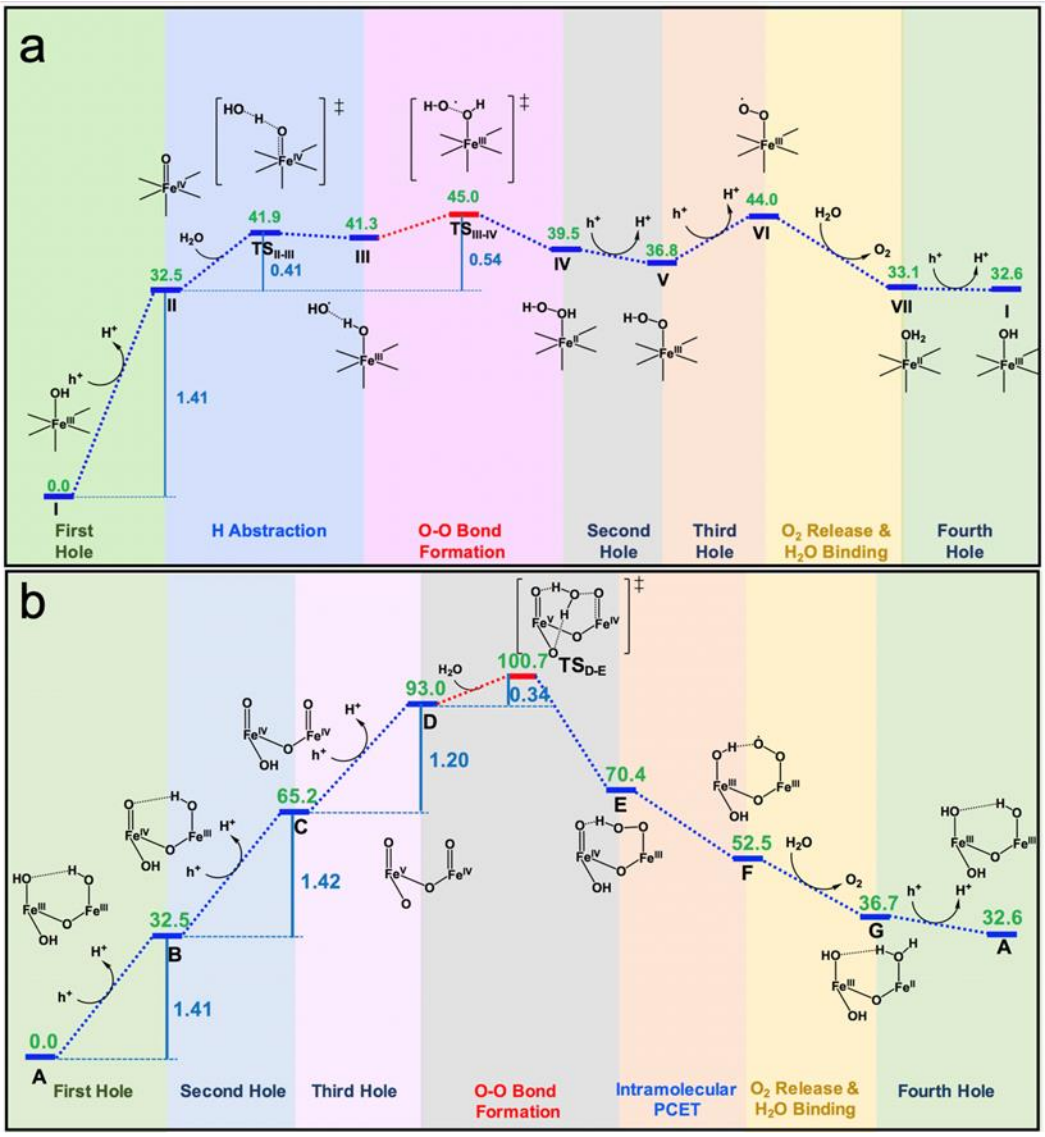
a
41.9
41.3
45.0
39.5
36.8
44.0
33.1
32.6
32.5
0.41
0.54
1.41
0.0
I
II
III
IV
V
VI
VII
I
First Hole
H Abstraction
O-O Bond Formation
Second Hole
Third Hole
O2 Release & H2O Binding
Fourth Hole
b
100.7
93.0
70.4
65.2
52.5
36.7
32.6
32.5
0.34
1.20
1.42
1.41
0.0
A
B
C
D
E
F
G
A
First Hole
Second Hole
Third Hole
O-O Bond Formation
Intramolecular PCET
O2 Release & H2O Binding
Fourth Hole

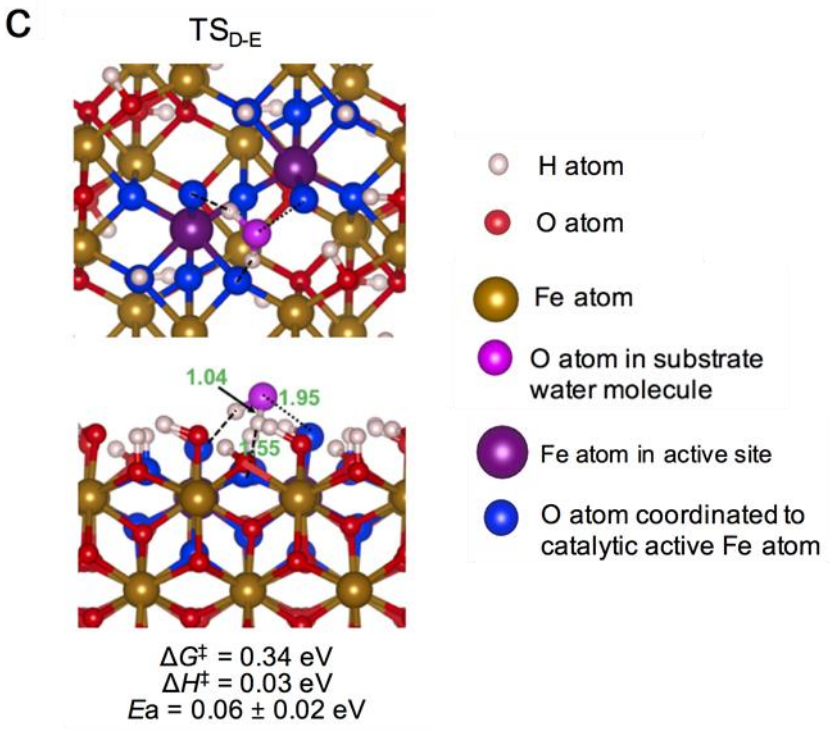


**Figure 3.** Potential water oxidation reaction mechanisms on $\alpha$-$Fe_2O_3$. (a) 1$^{st}$- and (b) 3$^{rd}$-order dependence kinetics, suggested by DFT calculations (Relative free energies are given in green in the unit of kcal/mol and free energy changes are given in blue in the unit of eV; rate-determining steps are shown in red: a photovoltage of 0.80 V is used for all oxidation steps). (c) Top view and side view of optimized transition state structures with key bond lengths given in the unit of Å. Dash lines indicate hydrogen bonds and dotted lines indicate partially formed bond s at transition states.

Density functional theory (DFT) studies were undertaken to provide insight into potential mechanisms of the observed 1$^{st}$ and 3$^{rd}$ order water oxidation kinetics. We note that the extensive literature on theoretical studies on the water oxidation mechanism on hematite[33–38] have focused primarily on the thermodynamic aspect with the kinetic data presented herein yet to be studied. We focus on the (110) surface of hematite, reported as the primary and most active facet for water oxidation, and the dominating facet of the photoelectrodes studied herein.[39,40] We employ a defect free surface, consistent with our experimental observation of surface hole densities being much greater than typical surface defect densities. We focus on a reaction site based on a hydroxyl terminated hematite (110) for which two neighbouring Fe(III)-OH groups form an Fe(OH)-O-Fe(OH) dimer in aqueous solutions (Figure 3.b and 3.c). Full details of the DFT calculations, including consideration of the hematite (110) surface/water interface, are given in the Supplementary Information.

We begin our discussion of the water oxidation mechanism corresponding to the observed 1$^{st}$ order kinetics. Oxidation of a surface $Fe^{III}$-OH leads to formation of $Fe^{IV}$=O, requiring an energy of 1.41 eV and consistent with a recent study by Zandi and Hamann,[30] which provided strong evidence for surface hematite holes comprising localised $Fe^{IV}$=O species. Under low illumination, and therefore low hole densities, the $Fe^{IV}$=O groups are isolated from each other. A potential pathway for water oxidation by such isolated surface holes is illustrated in Figure 3.a (see Supplementary Information for a detailed discussion). This mechanism is based upon the oxidation of an incoming substrate $H_2O$ molecule to form a hydroxyl radical, with the rate determining step of O-O bond formation having an activation free energy of 0.54 eV and enthalpy of 0.26 eV. This activation enthalpy is in agreement with our

experimental data for the 1st order reaction. The $H_2O_2$ intermediate (**IV**) after the rate determining step could be further oxidised to produce $O_2$ (Figure 3.a) or be released to the solution (see Supplementary Figure 11), with the former being thermodynamically more favourable. This mechanism is also consistent with our experimental data indicating only a weak pH dependence. Furthermore, the calculated H/D KIE associated with this mechanism is 1.03, again consistent with our experimental observation.

We now turn to consideration of the third order reaction mechanism, which dominates under one sun operating conditions. We analysed successive (and potentially reversible) oxidations of an Fe(OH)-O-Fe(OH) dimer core by neighbouring hematite surface valence band holes (Figure 3.b and Figure 4). Remarkably, the second and third oxidations of this dimer are thermodynamically similar to the first oxidation, with the third oxidation actually being the most facile. The second oxidation results in oxidation of the second $Fe^{III}$-OH to $Fe^{IV}$=O in the dimer, essentially corresponding to two nearest neighbour hematite surface holes. The third oxidation oxidizes one of the $Fe^{IV}$=O groups to $Fe^{V}$=O while deprotonating a surface OH group coordinated to the $Fe^{V}$ centre. After three successive oxidations, the Fe dimer gains enough oxidation power to drive the nucleophilic attack of an incoming substrate water molecule (Figure 3.c, $\mathbf{TS_{D\text{-}E}}$), and subsequent O-O bond formation. This O-O bond formation is relatively facile, requiring an activation free energy of only 0.34 eV and enthalpy of 0.03 eV (see Figure 3.c), in good agreement with our experimental observed activation enthalpy (0.06 eV). This reaction mechanism is consistent with our measurement of a modest KIE. In particular the rate determining step (rds) of O-O bond formation involves H atoms in the substrate water molecule (Figure 3.c, $\mathbf{TS_{D\text{-}E}}$), but does not involve O-H bond breaking. A similar KIE value has been reported for analysis of an analogous water oxidation mechanism on a ruthenium based molecular catalyst.[41] The calculated H/D KIE with $\mathbf{TS_{D\text{-}E}}$ is 2.5, which is consistent with our experimentally observed KIE of ~1.7, indicating a modest secondary H/D KIE. Similarly, the rds involves nucleophilic attack by a water molecule onto a Fe(IV)=O and does not directly involve hydroxide ions or proton release, consistent with the observed relatively weak pH dependence.

Mechanistic implications

The DFT calculations discussed above illustrate potential mechanisms for water oxidation consistent with our observed 1st and 3rd reaction kinetics. We now consider the more general implications of these experimental and theoretical data, focusing on the key 3rd order reaction pathway, as illustrated in Figure 4. A key element of this pathway is that three surface holes are in equilibrium with the triply oxidised cluster involved in the rds. The accumulation of three oxidising equivalents on a single cluster requires the lateral diffusion of surface holes, consistent with an analogous model previously proposed for $Co_3O_4$ by Frei and co-workers,[42] until three holes accumulate together to enable O-O bond formation. The subsequent steps leading to the $O_2$ release and $H_2O$ binding, and fourth oxidation, are thermodynamically downhill with no activation barrier.

The similarity of oxidation potentials for the 1st, 2nd and 3rd oxidations (redox levelling), as indicated by our DFT calculations, is analogous to that observed for oxidation of the oxomanganese complex of PS II[43,44] and for other catalytic systems such $RuO_2$.[45] As for PS II, an underlying redox levelling mechanism is likely essential to enable the accumulation of multiple oxidising equivalents at multi-metallic reaction sites. In both cases, this ability to drive multiple oxidations of a single cluster with similar driving energies results primarily from the proton release associated with the 1st, 2nd, and 3rd oxidations in our model, thus maintaining charge neutrality.

Our DFT calculations indicate the 1st, 2nd and 3rd oxidations of this cluster occur with similar oxidation potentials, without the need for consideration of any surface defects. This redox levelling can be attributed to proton release associated with each oxidation step, and is key to enabling the accumulation of three oxidising equivalents on the cluster. Such redox levelling associated with proton coupled electron transfer is also observed in the multi-metal oxygen evolution centre of Photosystem II.

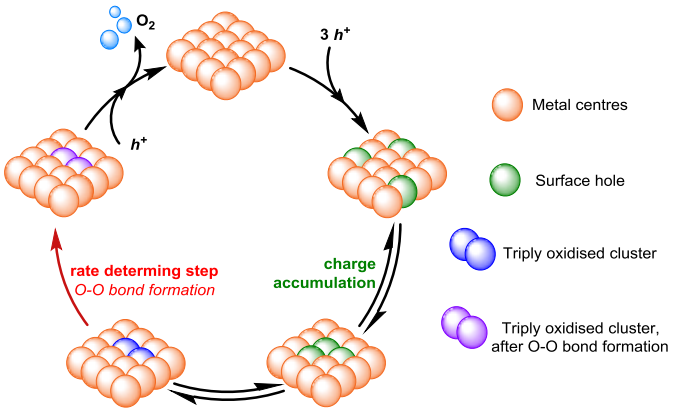


**Figure 4.** Schematic representation of the key steps in the 3rd order water oxidation reaction proposed herein. Equilibration between three surface holes and M(OH)-O-M(OH) sites is followed by O-O bond formation as the rate determining step, which is followed by a fourth oxidation and $O_2$ release.

Our observation of a modest acceleration of the rate constant at pH values greater than hematite's pzc, is consistent with the partial deprotonation of surface hydroxyls at a strongly alkaline pH. These deprotonated oxyl groups would provide effective proton transport channels to facilitate proton release from the oxidised cluster, thereby favouring the accumulation of multiple oxidation equivalents on a single dimer. Similarly, our observation of a modest increase in rate constant with VBE (Figure 1.c) could be explained by a shift of the equilibrium between three separated surface holes and the triply oxidised cluster towards the latter. This may also be associated with an increase in the surface hole reactivity for O-O bond formation.

The hematite photoelectrodes studied herein are very distinct in terms of system architecture and material/molecular composition from the biological water oxidation enzyme PS II. For example hematite undertakes the functions of both light absorber and catalyst, whilst in PS II these functions are separated between light absorbing pigments and a metal cluster based catalyst (the 'oxygen evolution complex' or 'OEC'). However, it is interesting to note that some of the fundamental aspects of the 3rd order water oxidation reaction mechanism proposed herein for hematite (and potentially for other metal oxides, as discussed below) have parallels to mechanisms proposed for oxygen evolving complex (OEC) of PSII. Both the proposed oxyl-oxo coupling pathway,[46,47] and the nucleophilic attack of a terminal oxyl radical by substrate water[48–52] for PS II require μ-oxo bridges linking the Mn metal centres in the OEC. These regulate the binding, deprotonation and oxidation of substrate water molecules as well as O-O bond formation processes, in ways analogous to those discussed herein for the hematite surface. For both systems, the thermodynamic coupling of oxidation and deprotonation events establishes a redox-levelling mechanism that enables low free energy pathways for the accumulation of multiple oxidising equivalents. For both systems, the accumulation of multiple oxidising equivalents in high-valent transition metal centres is necessary to induce deprotonation of water ligands and the formation of the reactive species responsible for O-O bond formation. On the other hand, clear differences are also apparent. The reaction mechanism proposed herein for

hematite proceeds via formation of a peroxo moiety, which contrasts to most models of water oxidation by PS II,[43,47,52–55] but has been proposed for heterogeneous water oxidation on other metal oxides such as $Co_3O_4$ or $IrO_2$.[56] It is also important to recognise that water oxidation on hematite (and the other oxides studied herein) proceeds with a slower turn over frequency and larger energetic driving energy than for PS II. Clearly, the OEC of PS II is a far more complex and effective catalyst for water oxidation than the relatively unsophisticated metal oxide surfaces studied herein. As such, it is remarkable that parallels can be drawn between water oxidation by these two very distinct systems, indicating that studies of natural water oxidation may indeed provide guidelines to aid further development of artificial heterogeneous water oxidation catalysts.

Our observation of similar for water oxidation rate laws for four different oxides suggests broadly similar reaction mechanisms on all four oxides. A full analysis of this issue is however beyond the scope of this study, with detailed specific reaction mechanisms likely to depend for example on oxide surface facet and the nature of surface holes. We note the water oxidation models proposed herein for hematite show common features with analogous reaction mechanisms proposed for other metal oxides. In particular Frei *et al.*[57] have reported the observation of distinct reaction intermediates for 'slow' and 'fast' water oxidation reactions on cobalt oxides, with proposed reaction mechanisms broadly consistent with the two 1$^{st}$ and 3$^{rd}$ order reaction mechanisms proposed herein. From the plausible mechanisms of 1$^{st}$ and 3$^{rd}$ order kinetics suggested by our DFT calculations, it is also possible that the participation of multiple nearby M-OH groups, as detailed in our 3$^{rd}$ order mechanism, is a common feature for efficient water oxidation on metal oxide surfaces. We note that both cobalt oxide and hematite have M(OH)-O-M(OH) sites, which can be oxidised by sequential proton coupled oxidations to accumulate enough oxidation power. These M(OH)-O-M(OH) sites are not only present on most metal oxides, but also in recently developed highly active homogeneous Ir and Fe based catalysts[58,59] and in the $Fe(IV)_2$ diamond-core structure of carboxylate-rich, non-heme diiron enzyme systems,[60–62] suggesting their importance for the development of efficient catalysts for water oxidation.

**Acknowledgements**

J.R.D. acknowledges financial support from the European Research Council (project Intersolar 291482) and H2020 project A-LEAF (732840). C.A.M thanks COLCIENCIAS (call 568) for funding, L.F. thanks the EU for a Marie Curie fellowship (658270) and E.P. thanks the EPRSC for a DTP scholarship. V. S. B. acknowledges support from the Center for Light Energy Activated Redox Processes (LEAP), an Energy Frontier Research Center funded by the U.S. Department of Energy, Office of Science, Office of Basic Energy Sciences, under Award Number DE-SC0001059 and high performance computing time from NERSC and Yale Center for Research Computing. A.K. thanks Imperial College for a Junior Research Fellowship. M.G. acknowledges Swiss National Science Foundation (project: 140709) and Swiss Federal Office for Energy (project: PECHouse 3, contract number SI/500090–03). T.E.R thanks the EPSRC for a DTC studentship and E.R. the Christian Doppler Research Association (Austrian Federal Ministry of Science, Research, and Economy and the National Foundation for Research, Technology and Development) and the OMV Group for financial support. M.T.M. acknowledges the Helmholtz Association's Initiative and Networking Fund.

**Author contributions**

C. A. M. and L. F. contributed equally to this work. All authors discussed the results, commented and revised the manuscript. C. A. M., L. F. and J. R. D. conceived, designed the experiments. K. R. Y., P. G.

and V. S. B. contributed the density functional theory work. E. P., Y. M., A. K., T. E. R., M. T. M., E. R. and M. G., contributed with materials and data.

**Competing interests**

The authors declare no competing interests.

**Data availability**

The complete optical and electrochemical data set is available in http://zenodo.org with the identifier (10.5281/zenodo.851635).

**References**


1. Zhu, S. & Wang, D. Photocatalysis: Basic Principles, Diverse Forms of Implementations and Emerging Scientific Opportunities. *Adv. Energy Mater.* 1700841 (2017). doi:10.1002/aenm.201700841
2. Berardi, S. *et al.* Molecular artificial photosynthesis. *Chem. Soc. Rev.* **43,** 7501–7519 (2014).
3. Walter, M. G. *et al.* Solar Water Splitting Cells. *Chem. Rev.* **110,** 6446–6473 (2010).
4. Lewis, N. S. & Nocera, D. G. Powering the planet: chemical challenges in solar energy utilization. *Proc. Natl. Acad. Sci. U. S. A.* **103,** 15729–35 (2006).
5. Sun, K. *et al.* A comparison of the chemical, optical and electrocatalytic properties of water-oxidation catalysts for use in integrated solar-fuel generators. *Energy Environ. Sci.* **10,** 987–1002 (2017).
6. Mccrory, C. C. L., Jung, S., Peters, J. C. & Jaramillo, T. F. Benchmarking Heterogeneous Electrocatalysts for the Oxygen Evolution Reaction. *J. Am. Chem. Soc.* **135,** 16977–16987 (2013).
7. Kärkäs, M. D. & Åkermark, B. Water oxidation using earth-abundant transition metal catalysts: opportunities and challenges. *Dalt. Trans.* **45,** 14421–14461 (2016).
8. Blakemore, J. D., Crabtree, R. H. & Brudvig, G. W. Molecular Catalysts for Water Oxidation. *Chem. Rev.* **115,** 12974–13005 (2015).
9. Llobet, A. *Molecular water oxidation catalysis: A key topic for new sustainable energy conversion schemes*. (John Wiley & Sons Ltd).
10. Dau, H. *et al.* The Mechanism of Water Oxidation: From Electrolysis via Homogeneous to Biological Catalysis. *ChemCatChem* **2,** 724–761 (2010).
11. Shinagawa, T., Garcia-Esparza, A. T. & Takanabe, K. Insight on Tafel slopes from a microkinetic analysis of aqueous electrocatalysis for energy conversion. *Sci. Rep.* **5,** 13801 (2015).
12. Gerischer, H. The Impact of Semiconductors On The Concepts Of Electrochemistry. *Electrochim. Acta* **35,** 1677–1699 (1990).
13. Francàs, L., Mesa, C. A., Pastor, E., Le Formal, F. & Durrant, J. R. *Chapter 5: Rate Law Analysis of Water Splitting Photoelectrodes*. *RSC Energy and Environment Series* (2018). doi:10.1039/9781782629863-00128
14. Pastor, E. *et al.* Spectroelectrochemical analysis of the mechanism of (photo)electrochemical hydrogen evolution at a catalytic interface. *Nat. Commun.* **8,** 14280 (2017).
15. Mesa, C. A. *et al.* Kinetics of Photoelectrochemical Oxidation of Methanol on Hematite

Photoanodes. *J. Am. Chem. Soc.* **139,** 11537–11543 (2017).

16. Le Formal, F. *et al.* Rate Law Analysis of Water Oxidation on a Hematite Surface. *J. Am. Chem. Soc.* **137,** 6629–6637 (2015).

17. Ma, Y. *et al.* Rate Law Analysis of Water Oxidation and Hole Scavenging on a BiVO 4 Photoanode. *ACS Energy Lett.* 618–623 (2016). doi:10.1021/acsenergylett.6b00263

18. Kafizas, A. *et al.* Water Oxidation Kinetics of Accumulated Holes on the Surface of a TiO 2 Photoanode: A Rate Law Analysis. *ACS Catal.* **7,** 4896–4903 (2017).

19. Pesci, F. M., Cowan, A. J., Alexander, B. D., Durrant, J. R. & Klug, D. R. Charge Carrier Dynamics on Mesoporous WO3 during Water Splitting. *J. Phys. Chem. Lett.* **2,** 1900–1903 (2011).

20. Barroso, M., Pendlebury, S. R., Cowan, A. J. & Durrant, J. R. Charge carrier trapping, recombination and transfer in hematite ([small alpha]-Fe2O3) water splitting photoanodes. *Chem. Sci.* **4,** 2724–2734 (2013).

21. Roger, I., Shipman, M. A. & Symes, Ma. D. Earth-abundant catalysts for electrochemical and photoelectrochemical water splitting. *Nat. Rev. Chem.* **1,** (2017).

22. Rosser, T. E., Gross, M. A., Lai, Y.-H. & Reisner, E. Precious-metal free photoelectrochemical water splitting with immobilised molecular Ni and Fe redox catalysts. *Chem. Sci.* **7,** 4024–4035 (2016).

23. Zhang, Y. *et al.* Rate-Limiting O−O Bond Formation Pathways for Water Oxidation on Hematite Photoanode. *J. Am. Chem. Soc.* **ASAP,** (2018).

24. Schulze, M., Kunz, V., Frischmann, P. D. & Würthner, F. A supramolecular ruthenium macrocycle with high catalytic activity for water oxidation that mechanistically mimics photosystem II. *Nat. Chem.* **8,** 576–583 (2016).

25. Kafizas, A. *et al.* Optimizing the Activity of Nanoneedle Structured $WO_3$ Photoanodes for Solar Water Splitting: Direct Synthesis via Chemical Vapor Deposition. *J. Phys. Chem. C* **121,** 5983–5993 (2017).

26. Cowan, A. J., Leng, W., Barnes, P. R. F., Klug, D. R. & Durrant, J. R. Charge carrier separation in nanostructured TiO2 photoelectrodes for water splitting. *Phys. Chem. Chem. Phys.* **15,** 8772 (2013).

27. Ma, Y., Le Formal, F., Kafizas, A., Pendlebury, S. R. & Durrant, J. R. Efficient suppression of back electron/hole recombination in cobalt phosphate surface-modified undoped bismuth vanadate photoanodes. *J. Mater. Chem. A* **3,** (2015).

28. Wang, X. H. *et al.* Pyrogenic Iron(III)-Doped TiO 2 Nanopowders Synthesized in RF Thermal Plasma: Phase Formation, Defect Structure, Band Gap, and Magnetic Properties. *J. Am. Chem. Soc.* **127,** 10982–10990 (2005).

29. Wahlström, E. *et al.* Bonding of Gold Nanoclusters to Oxygen Vacancies on Rutile TiO2 (110). *Phys. Rev. Lett.* **90,** 026101 (2003).

30. Zandi, O. & Hamann, T. W. Determination of photoelectrochemical water oxidation intermediates on haematite electrode surfaces using operando infrared spectroscopy. *Nat. Chem.* **8,** (2016).

31. Cowan, A. J. *et al.* Activation Energies for the Rate-Limiting Step in Water Photooxidation by Nanostructured α-Fe2O3 and TiO2. *J. Am. Chem. Soc.* **133,** 10134–10140 (2011).

32. Kosmulski, M. pH-dependent surface charging and points of zero charge. IV. Update and new approach. *J. Colloid Interface Sci.* **337,** 439–448 (2009).

33. Aharon, E. & Toroker, M. C. The Effect of Covering Fe2O3 with a $Ga_2O_3$ Overlayer on Water Oxidation Catalysis. *Catal. Letters* **147,** 2077–2082 (2017).

34. Yatom, N., Elbaz, Y., Navon, S. & Caspary Toroker, M. Identifying the bottleneck of water oxidation by ab initio analysis of in situ optical absorbance spectrum. *Phys. Chem. Chem. Phys.* **19,** 17278–17286 (2017).

35. Seriani, N. Ab initio simulations of water splitting on hematite. *J. Phys. Condens. Matter* **29,** 463002 (2017).

36. Grave, D. A., Yatom, N., Ellis, D. S., Toroker, M. C. & Rothschild, A. The "Rust" Challenge: On the Correlations between Electronic Structure, Excited State Dynamics, and Photoelectrochemical Performance of Hematite Photoanodes for Solar Water Splitting. *Adv. Mater.* **30,** 1706577 (2018).

37. Nguyen, M.-T., Seriani, N. & Gebauer, R. Back Cover: Defective α-Fe2O3 (0001): An ab Initio Study. *ChemPhysChem* **15,** 3136–3136 (2014).

38. Zhang, X., Klaver, P., Van Santen, R., Van De Sanden, M. C. M. & Bieberle-Hütter, A. Oxygen Evolution at Hematite Surfaces: The Impact of Structure and Oxygen Vacancies on Lowering the Overpotential. *J. Phys. Chem. C* **120,** 18201–18208 (2016).

39. Kay, A., Cesar, I. & Grätzel, M. New Benchmark for Water Photooxidation by Nanostructured α-Fe2O3 Films. *J. Am. Chem. Soc.* **128,** 15714–15721 (2006).

40. Cornuz, M., Grätzel, M. & Sivula, K. Preferential Orientation in Hematite Films for Solar Hydrogen Production via Water Splitting. *Chem. Vap. Depos.* **16,** 291–295 (2010).

41. Yamada, H., Siems, W. F., Koike, T. & Hurst, J. K. Mechanisms of Water Oxidation Catalyzed by the cis,cis-[(bpy)2Ru(OH2)]2O4+ Ion. *J. Am. Chem. Soc.* **126,** 9786–9795 (2004).

42. Pham, H. H., Cheng, M.-J., Frei, H. & Wang, L.-W. Surface Proton Hopping and Fast-Kinetics Pathway of Water Oxidation on Co3O4 (001) Surface. *ACS Catal.* **6,** 5610–5617 (2016).

43. Askerka, M., Brudvig, G. W. & Batista, V. S. The O2 ‐Evolving Complex of Photosystem II: Recent Insights from Quantum Mechanics/Molecular Mechanics (QM/MM), Extended X‐ray Absorption Fine Structure (EXAFS), and Femtosecond X‐ray Crystallography Data. *Acc. Chem. Res.* **50,** 41–48 (2017).

44. Amin, M. *et al.* Proton-Coupled Electron Transfer During the S‐State Transitions of the Oxygen-Evolving Complex of Photosystem II. *J. Phys. Chem. B* **119,** 7366–7377 (2015).

45. Rossmeisl, J. *et al.* Electrolysis of water on oxide surfaces. *J. Electroanal. Chem.* **607,** 83–89 (2007).

46. Siegbahn, P. E. M. O-O Bond Formation in the S4 State of the Oxygen-Evolving Complex in Photosystem II. *Chem. - A Eur. J.* **12,** 9217–9227 (2006).

47. Siegbahn, P. E. M. Water oxidation mechanism in photosystem II, including oxidations, proton release pathways, O—O bond formation and O 2 release. *Biochim. Biophys. Acta* **1827,** 1003–1019 (2013).

48. Pecoraro, V. L., Baldwin, M. J., Caudle, M. T., Hsieh, W.-Y. & Law, N. A. A proposal for water oxidation in photosystem II. *Pure Appl. Chem.* **70,** 925–929 (1998).

49. Vrettos, J. S., Limburg, J. & Brudvig, G. W. Mechanism of photosynthetic water oxidation: combining biophysical studies of photosystem II with inorganic model chemistry. *Biochim. Biophys. Acta* **1503,** 229–245 (2001).

50. Sproviero, E. M., Gascó, J. A., Mcevoy, J. P., Brudvig, G. W. & Batista, V. S. Quantum Mechanics/Molecular Mechanics Study of the Catalytic Cycle of Water Splitting in Photosystem II. *J. Am. Chem. Soc.* **130,** 3428–3442 (2008).

51. Barber, J. A mechanism for water splitting and oxygen production in photosynthesis. *Nat. Plants* **3,** (2017).

52. Barber, J. 'Photosystem II: the water splitting enzyme of photosynthesis and the origin of oxygen in our atmosphere'. *Q. Rev. Biophys.* **49,** 14–1 (2017).

53. Li, X. & Siegbahn, P. E. M. Water Oxidation for Simplified Models of the Oxygen-Evolving Complex in Photosystem II. *Chem. - A Eur. J.* **21,** 18821–18827 (2015).

54. Klauss, A., Haumann, M. & Dau, H. Seven Steps of Alternating Electron and Proton Transfer in Photosystem II Water Oxidation Traced by Time-Resolved Photothermal Beam Deflection at Improved Sensitivity. *J. Phys. Chem. B* **119,** 2677–2689 (2015).

55. Vinyard, D. J. & Brudvig, G. W. Progress Toward a Molecular Mechanism of Water Oxidation in Photosystem II. *Annu. Rev. Phys. Chem.* **68,** 101–16 (2017).

56. Zhang, M. & Frei, H. Water Oxidation Mechanisms of Metal Oxide Catalysts by Vibrational Spectroscopy of Transient Intermediates. *Annu. Rev. Phys. Chem* **68,** 209–31 (2017).

57. Zhang, M., De Respinis, M. & Frei, H. Time-resolved observations of water oxidation intermediates on a cobalt oxide nanoparticle catalyst. *Nat. Chem.* **6,** 362–367 (2014).

58. Yang, K. R. *et al.* Solution Structures of Highly Active Molecular Ir Water-Oxidation Catalysts from Density Functional Theory Combined with High- Energy X‐ray Scattering and EXAFS Spectroscopy. *J. Am. Chem. Soc.* **138,** 5511–5514 (2016).

59. Gamba, I., Codolà, Z., Lloret-Fillol, J. & Costas, M. Making and breaking of the O-O bond at iron complexes. *Coord. Chem. Rev.* **334,** 2–24 (2017).

60. Tinberg, C. E. & Lippard, S. J. Dioxygen Activation in Soluble Methane Monooxygenase. *Acc. Chem. Res.* **280,** 280–288 (2011).

61. Shu, L. *et al.* An $Fe_2^{IV}O_2$ Diamond Core Structure for the Key Intermediate Q of Methane Monooxygenase. *Science (80-. ).* **275,** 515–518 (1997).

62. Friedle, S., Reisner, E. & Lippard, S. J. Current challenges of modeling diiron enzyme active sites for dioxygen activation by biomimetic synthetic complexes. *Chem. Soc. Rev.* **39,** 2768–2779 (2010).

TOC Figure

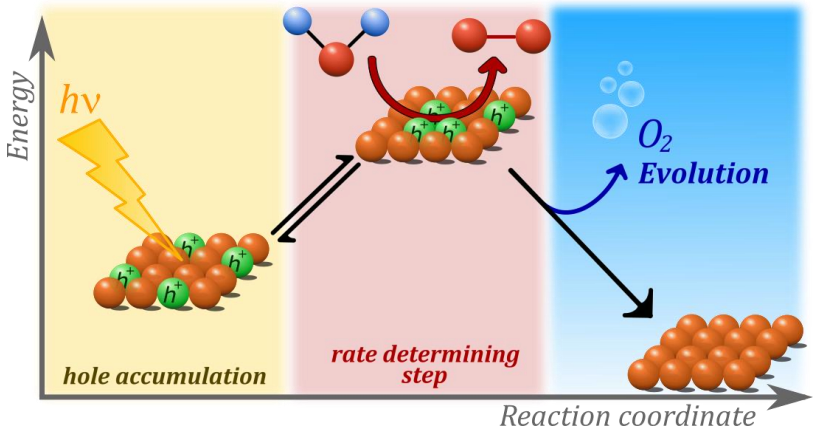


Figure captions

**Figure 1.** Kinetic analysis of the water oxidation reaction on metal oxide photoanodes. (a) Log/log plots of the turn over frequencies (TOF) for hole transfer to the electrolyte corresponding to water oxidation as a function of surface hole density, measured at fixed anodic bias for four metal oxide photoanodes. The black dashed circles indicate ~1 sun irradiation conditions. (b) Equivalent data plotted as rate of reaction versus surface hole density. The dashed lines correspond to fits to the rate law (Eq. 1). Conditions: $WO_3$, diffuse reflectance system ($\alpha$ = 1, $\alpha$ = 2.5), pH 3, applied potential 1.4 V vs RHE; $BiVO_4$, transmittance system ($\alpha$ = 1, $\alpha$ = 3), pH 7 at 1.7 V vs RHE;[17] $\alpha$-$Fe_2O_3$, transmittance system ($\alpha$ = 1, $\alpha$ = 3), pH 13 at 1.5 V vs RHE;[16] $TiO_2$, transmittance system ($\alpha$ = 3) pH 13 at 1.5 V vs RHE.[18] In all cases 365 nm LED irradiation was used from 0.5% to 300% one sun and measurements were performed at 25 $^{O}$C. (c) Schematic representation of the valence band edge energy relative to the $H_2O$ oxidation redox potential (1.23 V vs RHE) of the metal oxides discussed in this paper, including the equivalent PSII energy levels for reference.

**Figure 2.** Mechanistic analyses of water oxidation on $\alpha$-$Fe_2O_3$. (a) Rate law analyses as for Figure 1.b, but at different temperatures (21 °C – 50 °C). The inset shows an Arrhenius plot of water oxidation rate constant for both the 1$^{st}$ and 3$^{rd}$ order regimes, the slopes (dotted lines) indicate the activation energies of the rate determining steps, suggesting the catalytic effect of hole accumulation on $\alpha$-$Fe_2O_3$. (b) Plots of the pH dependence of the rate constants of the 1$^{st}$ and 3$^{rd}$ order regimes. (c) Comparison of the kinetic isotope effect when $H_2O$ is replaced by $D_2O$ at different pH values for the 3$^{rd}$ order (red) and 1$^{st}$ order (blue) regimes, exhibiting no cleavage of O-H bond at the rate determining steps. (b)-(c) Error bars represent the standard deviations of linear fits of the logarithmic form of equation 1 to the full data sets shown in Supplementary Figures 8 a and b.

**Figure 3.** Potential water oxidation reaction mechanisms on $\alpha$-$Fe_2O_3$. (a) 1$^{st}$- and (b) 3$^{rd}$-order dependence kinetics, suggested by DFT calculations (Relative free energies are given in green in the unit of kcal/mol and free energy changes are given in blue in the unit of eV; rate-determining steps are shown in red: a photovoltage of 0.80 V is used for all oxidation steps). (c) Top view and side view of optimized transition state structures with key bond lengths given in the unit of Å. Dash lines indicate hydrogen bonds and dotted lines indicate partially formed bond s at transition states.

**Figure 4.** Schematic representation of the key steps in the 3$^{rd}$ order water oxidation reaction proposed herein. Equilibration between three surface holes and M(OH)-O-M(OH) sites is followed by O-O bond formation as the rate determining step, which is followed by a fourth oxidation and $O_2$ release.